UNIVERSIDAD
COMPLUTENSE
MADRID

Universidad Complutense de Madrid

Facultad de Ciencias Físicas

Barcelona Supercomputing Center

Evaluation of initial conditions for predictions of ocean biogeochemistry

Trabajo Fin de Máster

Máster en Meteorología y Geofísica

Curso 2018 - 2019

Autor: Jaime Martín Agüí

Supervisores: Irene Polo Sánchez y Raffaele Bernardello

Abstract

The increasing concentration of atmospheric CO_2 has been largely studied as one of the main drivers of climate change. In order to simulate the Earth's future climate, it is crucial to accurately predict the evolution of carbon dioxide. To this end, sources and sinks of atmospheric carbon have to be precisely estimated. In this regard, the world's oceans represent one of the most important carbon sinks on the planet. Ocean physics is the main driver of carbon uptake on century-long timescales but, on shorter timescales (up to a decade), ocean biogeochemical processes like phytoplankton growth play a major role in driving natural fluctuations of ocean carbon uptake. In this research, reconstructions of surface chlorophyll *a* concentration (a proxy of phytoplankton biomass) were assessed against remote sensing observations. With the aim of finding the best set of initial conditions for near-term predictions of ocean biogeochemistry, four experiments generated from the ocean component of the EC-Earth earth system model were analysed. The four experiments differ in the way observations of temperature and salinity are assimilated. Large-scale and regional analysis evidence that the experiment a1z8 is the most suitable for predictions of chlorophyll *a*. This result was confirmed by the validation of simulated surface nutrient fields (NO_3) against climatological observations, pointing to the importance of including an appropriate region around the equator without any data assimilation. The experiments in which this region was wider led to the most realistic simulation of both variables. Driving the simulations towards a reference state in the equatorial region generates spurious processes that give rise to worse representations.

Contents

Introduction **3**

Data and methods **5**

- Satellite data 5

- Model description 6

  • Experiments 7

- Interpolation 8

- Metrics 9

Results **10**

- Large-scale analysis 10

- Regional analysis 13

- Correlation maps 18

Discussion **20**

Conclusions **21**

References **22**

Introduction

It is firmly established that one of the main drivers of climate change is the increasing concentration of greenhouse gases, primarily of carbon dioxide (CO_2), derived from human activities. The world's oceans currently take over about 25-30% of anthropogenic CO_2 from the atmosphere (Li et al., 2016). Furthermore, this carbon oceanic uptake seems to present temporal fluctuations in certain regions, as studied by Li et al (2016) for the North Atlantic and its relation with the NAO[1] at interannual and decadal timescales.

Near-term climate prediction (Fig. 1), ranging periods between 2 and 30 years, is an information tool for the climate adaptation and social progress, currently under development (Doblas-Reyes et al., 2013). It is based on two factors: internally generated variations, embracing different natural oscillation patterns, and forced variations, based on changes in the atmospheric composition, due to natural or anthropogenic processes. Therefore, an accurate prediction of atmospheric carbon dioxide scenarios could lead to a better understanding of the future climate. As stated above, carbon uptake by the oceans plays an important role in this matter. However, current changes in circulation and in the physical state of the oceans could alter this crucial capacity, resulting in an increase in the concentration of carbon dioxide in the atmosphere and an acceleration of climate change, referred to as the carbon feedback. Reliable predictions of ocean carbon uptake are, henceforth, of great interest and a source of predictability for climate predictions.

Phytoplankton takes up CO_2 at the ocean surface, through photosynthesis, and produces organic matter, part of which is exported to the deep ocean, in a process known as the biological pump. It is responsible for almost 50% of global photosynthesis, and plays a fundamental role in regulating the climate (Falkowski, 1996).

Chlorophyll *a* (Chl-a) is a good indicator of phytoplankton abundance. Therefore, its variability and its relation with different variables and events has been widely studied through observational data, using either *in situ* or remote sensing measurements: Pérez-Arvizu et al. (2013) analysed the seasonal variability of chlorophyll *a* and its response to *El Niño* conditions in the Gulf of California; Winder and Cloern (2010) examined the annual cycle of phytoplankton biomass through satellite chlorophyll data and its role as indicator of climate change.

Modelling studies of this and other biogeochemical variables have recently emerged, principally due to its importance in the future evolution of the climate system: Lee et al. (2014) looked into the response of chlorophyll concentration to *El Niño* events through an ocean-biogeochemical coupled model; Séférian et al. (2013) analysed the multiyear predictability of tropical marine productivity with an ESM[2].

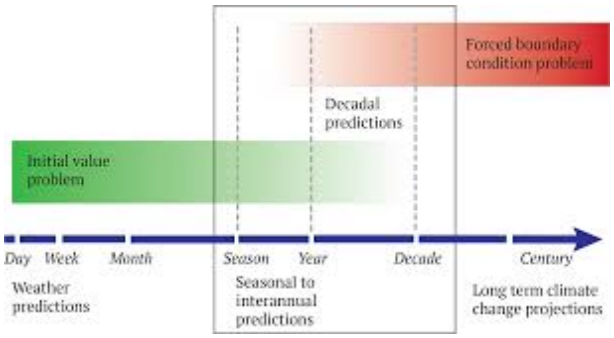

Fig. 1. Explanatory diagram of climate prediction. It takes into account initial conditions and long-term forcings. Source: `https://www.wcrp-climate.org`

In this research, the Chl-a variable simulated by the ocean component of the EC-Earth model was assessed through four different sets of initial conditions, generated with four reconstructions, each following a particular procedure of assimilation of observations for ocean temperature and salinity (nudging). The main objective of this project was to evaluate the solution of the biogeochemical model in response to the simulated ocean dynamics. This was done by

[1]North Atlantic Oscillation.
[2]Earth System Model.

validating simulated ocean surface chlorophyll against remote sensing observations. The outcome of this analysis indicates which of the four reconstructions is the most suitable to provide initial conditions to be used for predictions of ocean biogeochemistry.

The four reconstructions analyzed are simulations of the past oceanic conditions, also known as hindcasts. This is a way of testing numerical models, based on simulating past events and evaluating how well predictions match observational data (Doblas-Reyes et al., 2013).

Through this method, large-scale and regional analysis were carried out to find high skill spots, that is, areas where the model faithfully simulates the variable, and examining differences between the four experiments. Large-scale assessment was done globally and by hemispheres, with the equatorial region separately. The studied regions are illustrated in Fig. 2 and indicated in Table 1. The covered period runs from July 2002 to December 2015, with a monthly timestep.

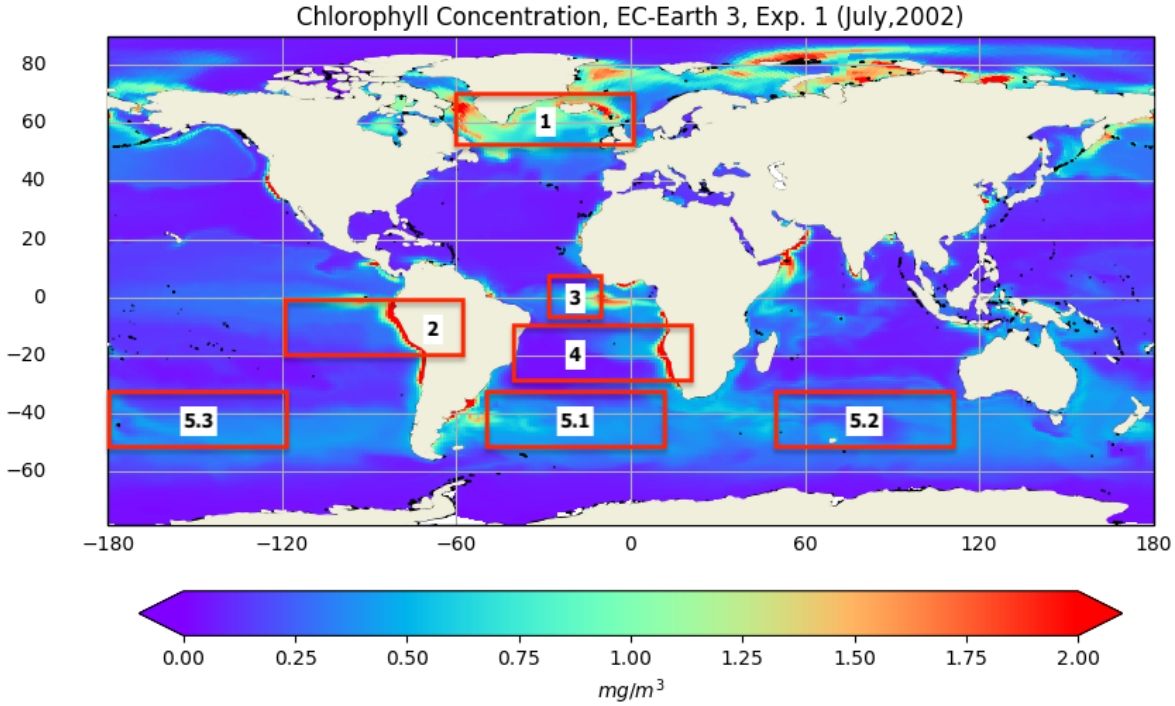

Fig. 2. Example of a Chl-a map from EC-Earth with the analysed regions.

Table 1. Analysed regions.

Region N.º	Region	Coordinates
1	North Atlantic Region	50ºN-70ºN, 0ºW-60ºW
2	Peruvian Region	0ºS-20ºS, 60ºW-120ºW
3	Equatorial Atlantic Region	7ºS-7ºS, 10ºW-30ºW
4	Namibian Region	10ºS-30ºS, 20ºE-40ºW
5	Southern Ocean Regions	
5.1	Southern Atlantic Region	35ºS-55ºS, 50ºW-10ºE
5.2	Southern Indian Region	35ºS-55ºS, 50ºE-110ºE
5.3	Southern Pacific Region	35ºS-55ºS, 120ºW-180ºW

Data and methods

Satellite data

Observational data is a crucial element in almost any kind of research. Particularly in Earth sciences, the amount and the quality of information largely determines the accuracy of an investigation. NASA's[3] Earth Observing System (EOS) is a program conceived in the 1990*s* with the aim of making progress on this issue. Aqua is one of the satellite missions arising from EOS, launched in May 2002. It is a near polar, sun-synchronous satellite, which means that its orbit combines altitude (705 km) and inclination (98.2°) so that it crosses the equator at the same local hour (1:30 $p.m.$ from south to north and 1:30 $a.m.$ from north to south). Aqua holds a stream of approximately 89 gigabytes of data every day, derived from six different instruments. Its main field of observation focuses on the water cycle, measuring evaporation, water vapor, clouds, soil moisture, etc. Furthermore, it also provides information about variables such as phytoplankton and biogeochemistry, among others. One of its measuring devices is the Moderate Resolution Imaging Spectroradiometer (MODIS). This is a medium resolution, 36-band spectroradiometer embracing wavelengths from 0.41 to 14.4 μm, dealing with spatial resolutions between 250 m and 1000 m and a global coverage every one to two days. MODIS provides information about numerous atmospheric, land-surface and oceanic features. The ocean color, phytoplankton and biogeochemistry are included in nine bands from 405 to 877 nm.

The essential quantity to be derived from ocean color sensors is the spectral distribution of reflected visible radiation upwelling from the ocean surface and passing through the sea-air interface (Gordon and Wang, 1994). However, satellite sensors measure the spectral radiance that reaches the Top Of the Atmosphere (TOA), which has spurious contributions from different origins that must be removed, such as light reflected by air molecules and aerosols or attenuating effects due to atmospheric gases and scattering. The Remote Sensing Reflectance algorithm (R_{rs}) carries out this atmospheric correction and estimates an accurate value of the spectral radiance upsurging from beneath the ocean surface, normalized by the downwards solar irradiance. The chlorophyll a algorithm (chlor_a) uses this R_{rs} output together with in situ measurements to derive an empirical relationship in the blue-to-green region of the visible spectrum to obtain the near-surface concentration of chlorophyll a.

The implementation of the chlor_a algorithm used in this research employs a combination of the standard Ocean Color (OC3) algorithm (O'Reilly et al., 2000), when the chlorophyll concentration is higher than 0.2 mg/m^3, and the Color Index (CI) algorithm (Hu et al., 2012), for concentrations below 0.15 mg/m^3. Between these two values, a weighted blend approach of both algorithms is used.

The OC3 is a three-band algorithm given by a fourth-order polynomial relationship between a ratio of R_{rs} and chlor_a, with sensor-specific coefficients (a_0-a_4):

$$log_{10}(chlor\_a) = a_0 + \sum_{i=1}^{4} a_i \left(log_{10} \left(\frac{R_{rs}(\lambda_{blue})}{R_{rs}(\lambda_{green})} \right) \right)^i$$

The CI is a three-band algorithm based on the difference between R_{rs} in the green band and a standard linear relation between R_{rs} in the blue and red bands:

$$CI = R_{rs}(\lambda_{green}) - [R_{rs}(\lambda_{blue}) + (\lambda_{green} - \lambda_{blue})/(\lambda_{red} - \lambda_{blue}) * (R_{rs}(\lambda_{red}) - R_{rs}(\lambda_{blue}))]$$

where λ_{blue}, λ_{green} and λ_{red} are the closest wavelengths to 443, 555 and 670 nm, respectively, for a given instrument.

The use of remote sensing for the estimation of ocean chlorophyll involves a certain error, especially in coastal areas, where turbidity may play an important role in the output of the previous algorithms (Chen et al., 2013). In order to roughly

[3]National Aeronautics and Space Administration.

correct this disparagement when comparing observation and simulated fields, chlorophyll concentration values greater than 20 mg/m^3 were considered spurious and removed.

Products obtained from this kind of sensors are processed at various levels, where level 0 represents raw data as obtained directly from the instrument. In this case, level 3 products were used. Variables are mapped on uniform space-time grid scales, within an equidistant cylindrical projection (Fig. 3). This spatial representation transforms the globe into a rectangular grid, in which each cell has the same size, shape and area, with a resolution of 4.6 km (8640 x 4320 longitude/latitude).

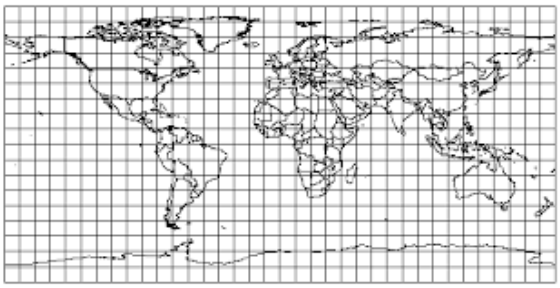

Fig. 3. Equidistant cylindrical projection. Source: `https://www.eye4software.com`

Remotely sensed data are sparse, which means that data have missing values, for instance due to cloud cover (Gerber et al., 2016). On the other hand, the simulations do not present this problem. To correctly analyse the data, after obtaining both fields on the same mesh, a mask was applied to each field with the missing values of the other. The validation is, therefore, more representative of the model's ability to predict this variable.

Model description

The four experiments that were evaluated in this study come from the ocean component of the EC-Earth model, concretely from its current version, EC-Earth 3. The EC-Earth model is a state-of-the-art numerical ESM based on the ECMWF's[4] seasonal forecasting system (Donners et al, 2012). It is formed by the IFS[5] for the atmosphere, NEMO[6] for the ocean, the land module HTESSEL[7] built in IFS and the LIM[8] sea ice model, which is part of NEMO.

One of the modules available in NEMO is PISCES[9]. This is a biogeochemical model which simulates the lower trophic levels of marine ecosystems (phytoplankton, microzooplankton and mesozooplankton) and the biogeochemical cycles of carbon and of the main nutrients (P, N, Fe, and Si). The amount of these nutrients limits the growth of phytoplankton, that is divided into two classes, nanophytoplankton and diatoms, with different requirements. For both groups, the prognostic variables are carbon, iron and chlorophyll biomasses, including silicon biomass only for diatoms (Aumont et al., 2015). These variables are presented on a global mesh called ORCA (Fig. 4). This is an ocean non-regular tripolar grid, which means that the north pole is divided in two land points (Asia and Canada), in order to cover the whole ocean domain avoiding any singularity point.

Fig. 4. Curvilinear tripolar grid (ORCA). Source: `https://www.geomar.de`

[4]European Centre for Medium-Range Weather Forecast.
[5]Integrated Forecasting System.
[6]Nucleus for European Modelling of the Ocean.
[7]Hydrology in the Tiled ECMWF Scheme for the Surface Exchange over Land.
[8]Louvain-La-Neuve Ice Model.
[9]Pelagic Interactions Scheme for Carbon Ecosystem Studies.

There are different configurations for ORCA, depending on the horizontal resolution. The one used in this simulations is ORCA1, in which the resolution at the equator is 1 degree, with a meridional refinement down to 1/3 degree in the tropics (362 x 292 longitude/latitude) and 75 vertical levels. Only the surface level was used in this dissertation, as this data was compared against satellite measurements from the reflected surface radiation.

Experiments

Newtonian relaxation or nudging is a simple form of data assimilation commonly used in meteorological modelling. It involves adding artificial forcing terms to the governing equations, that reflect the difference between the model and the observed values, driving the simulation towards a reference state (Otte, 2007). Although it may seem optimal to introduce large corrections to guide the model output, there are several drawbacks to this, as studied Ortega et al. (2017).

In this case, 3D nudging was applied, as indicated by the third column in Table 2. This refers to the relaxation timescales used for the interior ocean, affecting temperature and salinity below the mixed layer. This values are additionally multiplied by a depth-dependent constant (relaxation constant, τ), which allows to modify the speed at which the solution approaches the reference value.

In addition, surface restoring was employed for the upper part of the ocean, which relies on the assumption that the ocean mixed layer can be initialised through a proper representation of relevant processes forced by the ocean surface (Ortega et al., 2017). The main advantage of this technique is the availability of ocean surface data compared to lower levels. Surface restoring is classically done by adding heat and freshwater fluxes to the energy and salinity conservation equations. The heat flux is given by γ_T (associated with SST_{model}[10] $- SST_{target}$) and the freshwater flux is given by γ_S (associated with SSS_{model}[11] $- SSS_{target}$). Furthermore, there is a no-nudging band around the equator, since this is a very dynamic region and it is not convenient to force it. The four experiments used in this research differ in these parameters, as shown in Table 2.

Table 2. Nudging parameters for the four experiments. k represents a relaxation scale that determines τ and *M.L.* refers to the mixed layer depth.

Exp. N.º	Exp. ID	Relaxation constant	Surface restoring	No-nudging
1	a1yp	**Default:** τ(k=2 ⇔ z=1.5m) = 3 days τ(k=10 ⇔ z=14m) = 3.1 days τ(k=20 ⇔ z=61m) = 3.2 days τ(k=30 ⇔ z=180m) = 3.8 days τ(k=40 ⇔ z=500m) = 5.6 days τ(k=46 ⇔ z=950m) = 9.2 days τ(k=50 ⇔ z=1390m) = 15.4 days τ(k=60 ⇔ z=3000m) = 84 days τ(k=70 ⇔ z=4900m) = 329 days	**Default:** $\gamma_T = -40\ W/m^2/K$ $\gamma_S = -150\ mm/day$	3ºS - 3ºN
2	a1z8	τ(M.L.< z < 800m) = 10 days τ(z > 800m) = 360 days	**Default**	15ºS - 15ºN
3	a1zs	**Default**	$\gamma_T = -600\ W/m^2/K$ $\gamma_S = -2250\ mm/day$	3ºS - 3ºN
4	a20w	**Default**	**Default**	6.4ºS - 6.4ºN

[10]Sea Surface Temperature.
[11]Sea Surface Salinity.

Interpolation

The first step for the model validation was to obtain both fields on the same mesh. In this study, the low resolution model field was transformed into the high resolution grid of the satellite data, due to the massive presence of missing values in the observations. This method has to be carefully used for small-scale studies, as increasing the model resolution could lead to unrealistic values. Nevertheless, the purpose of this research ranges from considerably large regions to global analysis.

In the model field, inland regions were filled as missing values (NaNs[12]). This fact leads to a loss of information in coastal areas due to the interpolation. With the aim of improving this issue, all the missing values of every map were replaced by its zonal mean before the interpolation, and removed afterwards. An ordinary linear interpolation was then carried out.

To ensure the validity of the interpolation, several aspects were checked. The most important one was the conservation of the global quantity of chlorophyll. For this purpose, both fields had to be weighted by the grid element area, assuming that the total area of both grids was the same (the total area of the original grid was 0.8% lower than the interpolated one, as shown in Table 3). The global sum of the weighted variable had to be similar in both cases.

Before calculating this quantity, it was necessary to eliminate the unreal chlorophyll previously introduced in the continental regions, with the complication of locating these points on the interpolated map. To this end, a binary map was generated from the original field, differentiating between inland and oceanic regions (Fig. 5a). This map was then interpolated by the nearest method (returns the value at the data point closest to the point of interpolation), obtaining the continents in the new grid (Fig. 5b).

As shown in Fig. 5, the interpolation seems to be consistent while dealing with missing values, so it was possible to apply this mask to the interpolated field and compare the global sum of the weighted variable. In this way, the obtained results (Table 3), for an arbitrary time, allowed to assume the validity of the interpolation method. The global sum of chlorophyll was 0.7% higher for the original field than for the interpolated field. Other interpolation methods were tested and this one offered the most accurate results.

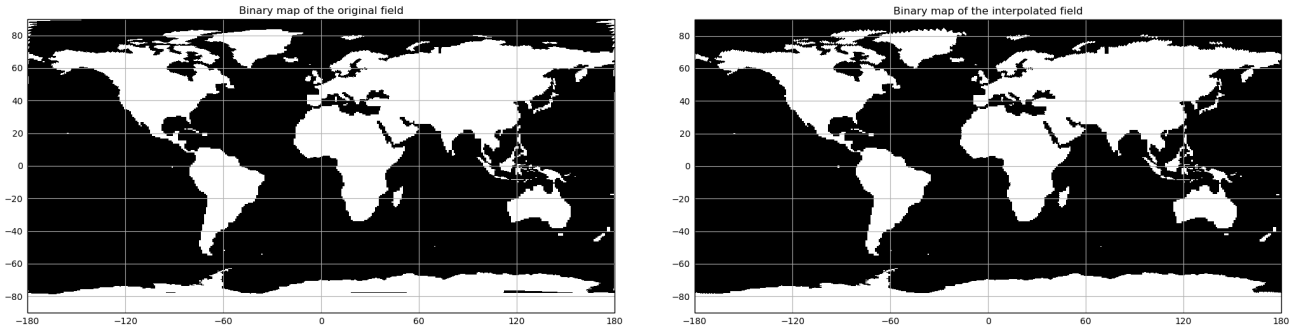

(a) (b)

Fig. 5. Continental regions from the original field (5a) were interpolated through a binary map by the nearest method, obtaining the continental regions in the interpolated map (5b).

[12]Not a Number.

Table 3. Interpolation assessment results.

	Original field	Interpolated field
Maximum value (mg/m^3)	4.2049	4.1751
Minimum value (mg/m^3)	0	0
Global mean (mg/m^3)	0.1791	0.1715
N.º of points	105704	37324800
N.º of NaNs	40160	12743345
Ratio Points/NaNs	2.632	2.929
Original/interpolated total grid area	0.992	
Original/interpolated chlorophyll global sum	1.007	

Metrics

There are many indices used for validating numerical models. Each one has specific characteristics and has to be correctly interpreted. In this research, four different metrics were calculated while comparing simulated data against observations:

– Pearson's correlation coefficient (r): measure of the linear dependence between two variables. It has a value between +1 (perfect direct correlation) and −1 (perfect inverse correlation), where 0 represents a null correlation.

$$\boxed{r = \frac{\sigma_{xy}}{\sigma_x \cdot \sigma_y}}$$

$$\sigma_{xy} = \frac{1}{n} \cdot \sum_{i=1}^{n} (x_i - \bar{x}) \cdot (y_i - \bar{y})$$

$$\sigma_x = \sqrt{\frac{1}{n} \cdot \sum_{i=1}^{n} (x_i - \bar{x})^2}$$

Where x refers to predictions, y to observed values, $\bar{x}$ is the mean of x (the same for $\bar{y}$), n is the number of data, σ_{xy} is the covariance between x and y and σ_x is the standard deviation of x (the same for σ_y).

– Root Mean Square Error ($RMSE$): measures the mean quadratic value of the error, which means that it heavily weights values away from the mean value. Its lower value is 0, when the predictions are exactly the same as the real data. It has the same units as the analysed variable.

$$\boxed{RMSE = \sqrt{\frac{1}{n} \cdot \sum_{i=1}^{n} (x_i - y_i)^2}}$$

– Mean Absolute Error (MAE): measures the average magnitude of the error between the observations and the data estimated by the model. All the individual differences are equally weighted. Its lower value is 0, when the predictions are exactly the same as the real data. It has the same units as the analysed variable.

$$\boxed{MAE = \frac{1}{n} \cdot \sum_{i=1}^{n} \mid x_i - y_i \mid}$$

– Mean Error or bias (ME): measures whether the model overestimated or underestimated the observational data. A null value does not imply a perfect correspondence with the observations, as positive and negative errors can be compensated. It has the same units as the analysed variable.

$$\boxed{ME = \frac{1}{n} \cdot \sum_{i=1}^{n} (x_i - y_i)}$$

Results

The following results represent two types of analysis. On one hand, temporal series of the monthly spatial mean surface chlorophyll *a* concentration (SCC onwards). In this case, the metrics indicate how the model captures the temporal variability of the averaged SCC. On the other hand, temporal series of the spatial metrics. This shows the ability of the model to predict the spatial distribution of the variable and the temporal variation of this skill. Both reviews are used either in large-scale and regional analysis.

Large-scale analysis

As a starting point, the spatial mean and variance of the variable was globally calculated for every month of the studied period, for both observations and experiments (Fig. 6). This gives an overview of the accuracy of the model to predict the variability of the SCC. At these scales, the experiments barely differ, so they were averaged for the analysis.

The model adequately reflects the seasonal cycle of chlorophyll, with a significant Pearson's correlation coefficient of 0.68 ($p\text{-}value < 0.05$), although it does not capture the marked increase in SCC observed during the last two years of the analysed period (2014-2015). Furthermore, it is clear that the model does not capture the spatial dispersion of the variable, as it presents a considerably low variance compared to the observational data. The simulated fields present also lower temporal variability, as showed by the standard error bars in Fig. 7.

Monthly averages for the whole period show that the highest global SCC occurs during the northern summer. However, the model underestimates the variable during the months of high SCC and overestimates it during the months of low SCC, that is, it presents a less pronounced seasonal pattern.

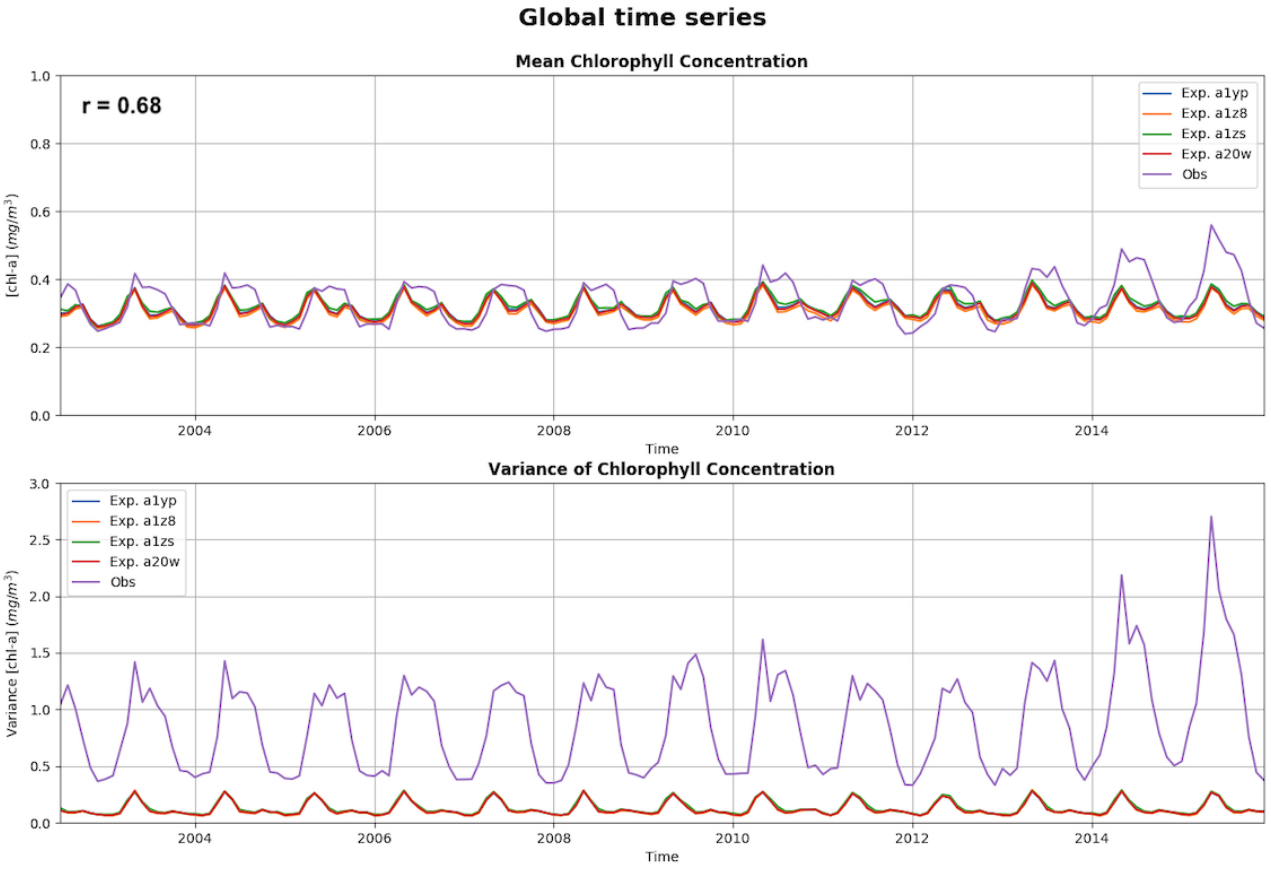

Fig. 6. Global time series of the spatial mean and variance of SCC for both observations and experiments. r represents the temporal correlation between the observations and the average of the four experiments.

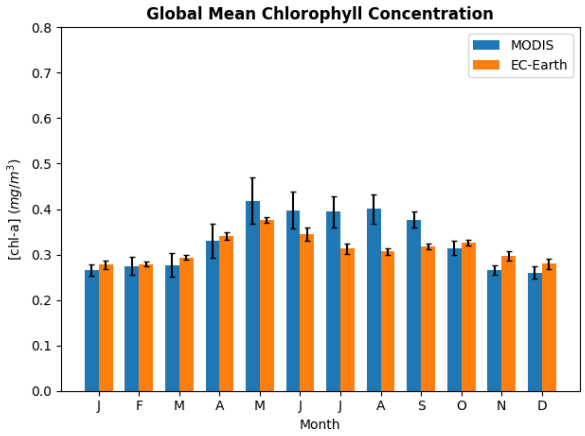

Fig. 7. Global monthly averages (± standard deviation) over the analysed period for the observations and the average of the four experiments.

The same procedure was followed for both hemispheres and the equatorial region (10°N-10°S) separately. As studied by Yoder et al. (1993), among others, the Northern Hemisphere (NH) presents higher SCC values than the Southern Hemisphere (SH), and also a stronger seasonal cycle (Fig. 9). The NH presents the same SCC increase over the last two years, as previously observed globally.

The model reasonably predicts the variable for the NH ($r = 0.54$). However, it is also remarkable that the high SCC period in this hemisphere lasts for a few months (April, May, June, July, August and September) while the model just captures it for April and May, widely underestimating the variable the following months. In the SH, the model shows an unreal seasonal pattern, where the measured SCC is almost constant through time ($r = 0.43$). This spurious oscillation corresponds to higher SCC values during the summer months, as found for the NH. Yet, satellite data does not present this pattern significantly in the SH.

As expected from the variable no-nudging bands of the experiments and contrary to both hemispheres, the equatorial region shows differences between the four experiments. Although the correlation coefficient is really similar for all of them ($r \sim 0.75$), the bias of each experiment varies. Experiment a1z8 presents the lowest error (Table 4).

Table 4. Root mean square error of each experiment for the equatorial region.

Experiment	RMSE (mg/m^3)
1. a1yp	0.047
2. a1z8	**0.025**
3. a1zs	0.053
4. a20w	0.034

Monthly averages (Fig. 10) show that the model underestimates the SCC in the NH and overestimates it in the SH for every month, while it accurately predicts it in the equatorial region. As stated above, the SH is much more homogeneous than the NH, not only spatially but also temporally, as evidenced by the standard deviations presented in Fig. 10.

Apart from the temporal correlation of the spatial mean series, the spatial correlation was calculated map to map, obtaining the temporal series of the corresponding coefficient. The global spatial correlation (Fig. 8) presents a seasonal pattern, ranging approximately from r=0.2 to r=0.5, contrary to that of the global mean SCC, that is, the model is less precise during the high SCC months. There is a subtle increase in the maximum and minimum correlation coefficient for the last three years of the analysed period. There are no noticeable differences between the experiments on the global scale.

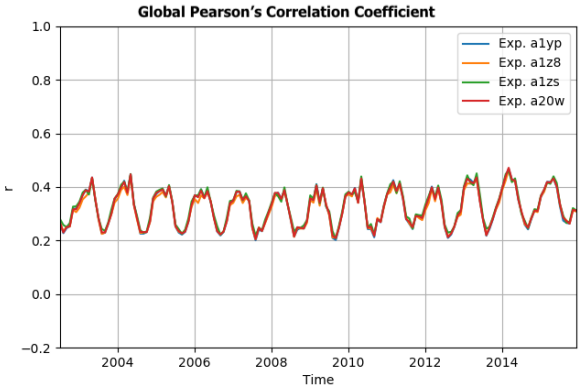

Fig. 8. Global spatial correlation series for each experiment.

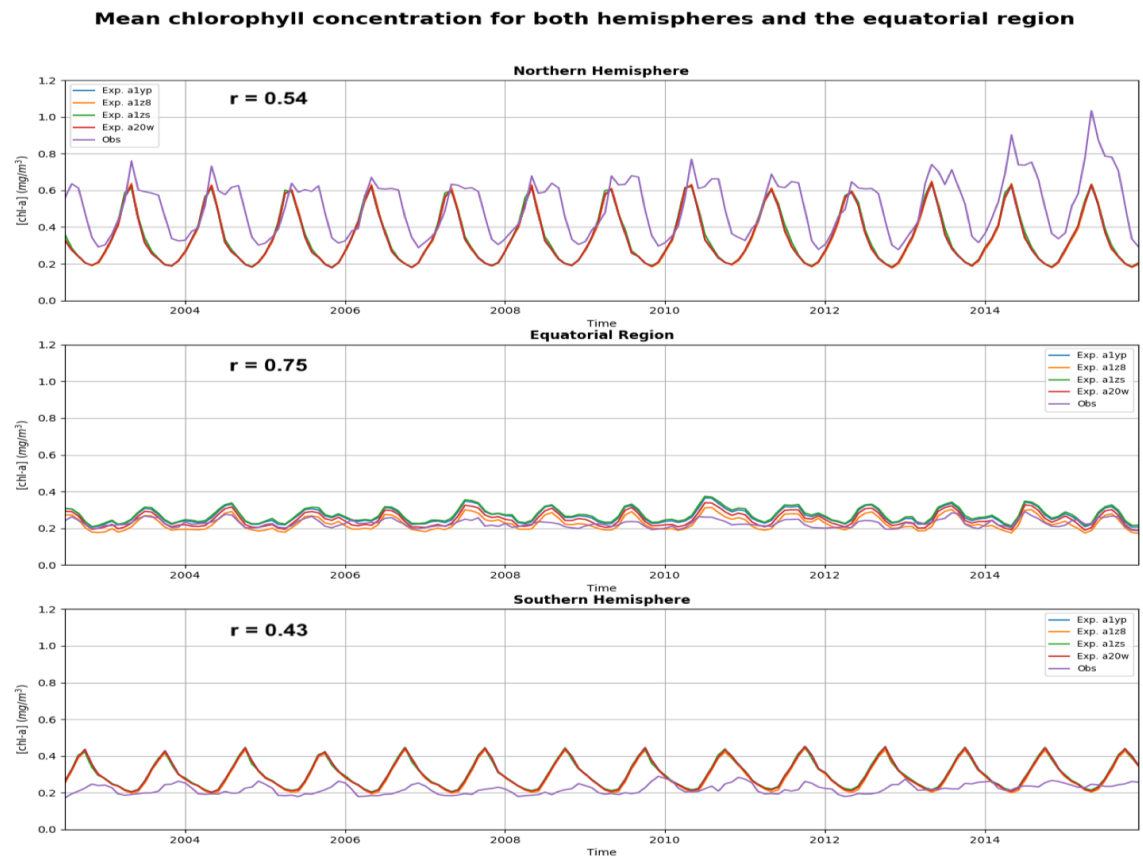

Fig. 9. Time series of the spatial mean of SSC for both hemispheres and the equatorial region, either for the observations and the experiments. r is referred to the temporal correlation between the observational data and the averaged series of the four experiments.

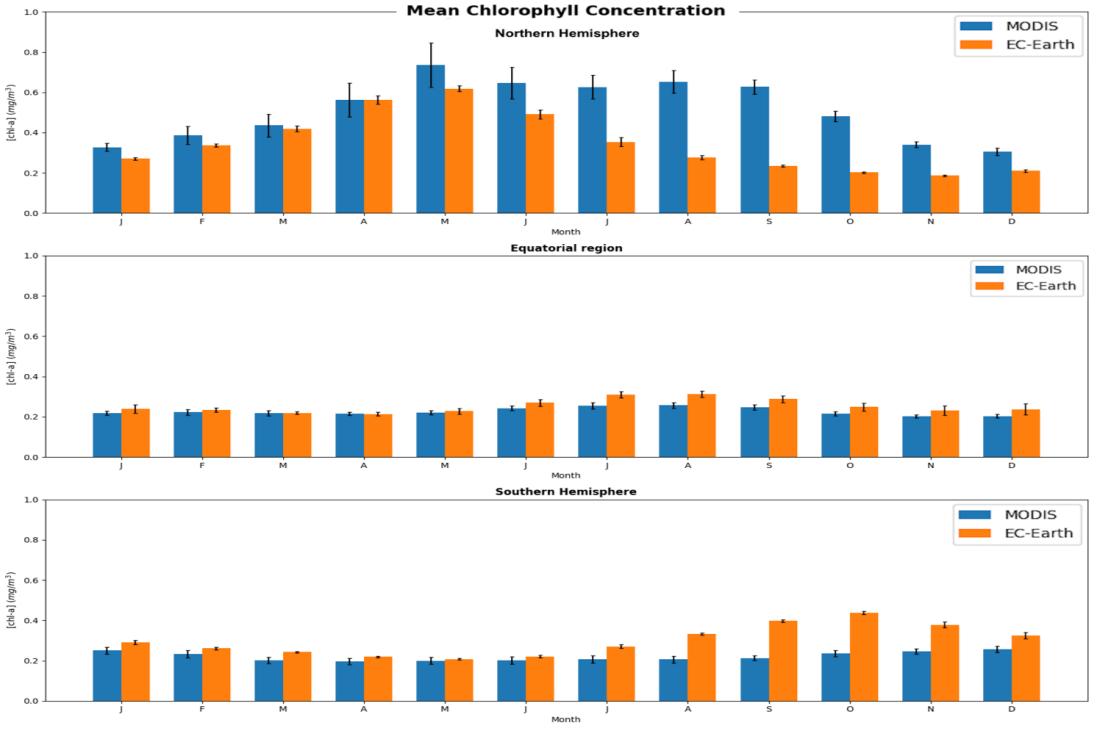

Fig. 10. Monthly averages of SCC (± standard deviation) for both hemispheres and the equatorial region (10°N-10°S) over the analysed period for the observations and the mean of the four experiments.

Regional analysis

In order to assess the skill of the model and the differences between the experiments at lower spatial scales, some key regions were selected for the analysis (Fig. 2). The accuracy of the simulations at these scales shows the capacity of the model to predict the spatial and temporal variability of high concentration areas and the influence of the different nudging parameters on it.

1. *North Atlantic Region*

This region presents a really accused seasonal cycle, with high SCC during the boreal summer months, as studied by Winder and Cloern (2010). There is no data for November and December, as the satellite can not measure in high latitudes during the winter due to low light conditions. It is remarkable the increase in observational values during 2014 and 2015, as observed for the global and hemispheric series. As in the other cases, the model does not capture this variation (Fig. 12).

There are almost no differences between the experiments in this region. The temporal correlation of the spatial mean SCC series (Fig. 12) was then calculated for the average of the four experiments, obtaining a Pearson's correlation coefficient of 0.71.

The spatial correlation series (Fig. 11) indicates that the model simulates the variable with considerable precision (r values up to 0.8) during the low SCC months, but hugely reduces its skill during the high SCC period (r values near 0 or even negative). The third experiment (a1zs) shows slightly lower correlations than the rest for certain months.

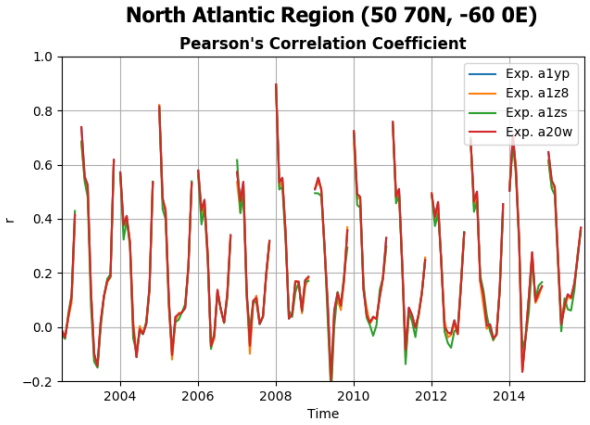

Fig. 11. Time series of the spatial correlation in the North Atlantic region for each experiment.

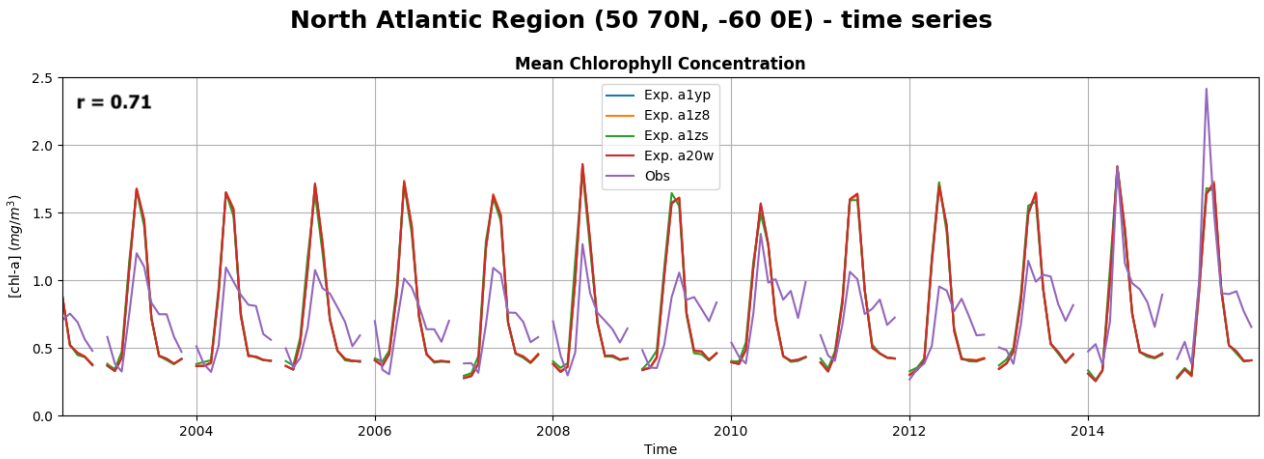

Fig. 12. Time series of the spatial mean SCC in the North Atlantic region for each experiment and observations. r is referred to the temporal correlation between the observational data and the average series of the four experiments.

2. *Peruvian Region*

The observed mean SCC (Fig. 13) shows a very subtle seasonal variability, with higher values during austral summer months, around 0.3 mg/m^3, in phase opposition with coastal upwelling intensity, as studied by Echevin et al. (2008) and low values during the winter, around 0.2 mg/m^3. The model exhibits just an opposite pattern, as the high SCC period is displaced to NH summer months. This fact is reflected in the temporal correlation coefficient, with a significant negative value of -0.18 (p-*value*<0.05), for the average of all the experiments. Although the four experiments overestimate the SCC, there are appreciable differences in the bias between them (Table 5). Experiment a1z8 presents the lowest error.

Table 5. Root mean square error of each experiment for the Peruvian region.

Experiment	RMSE (mg/m^3)
1. a1yp	0.22
2. a1z8	**0.17**
3. a1zs	0.24
4. a20w	0.20

On the other hand, the spatial correlation in this region varies, coarsely, between 0.4 and almost 0.8 (Fig. 14). Therefore, even though the temporal variability of the monthly SCC average is not correctly simulated, the spatial distribution of the variable in this area is well captured by the model. As in the spatial mean series, the second experiment presents the lowest mean error values.

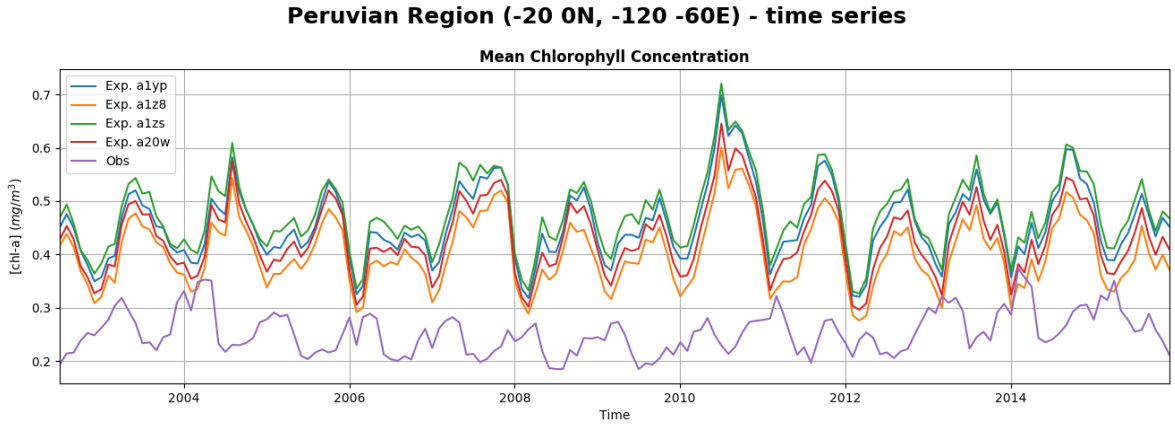

Fig. 13. Time series of the spatial mean SCC in the Peruvian region for each experiment and observations. r is referred to the temporal correlation between the observational data and the average series of the four experiments.

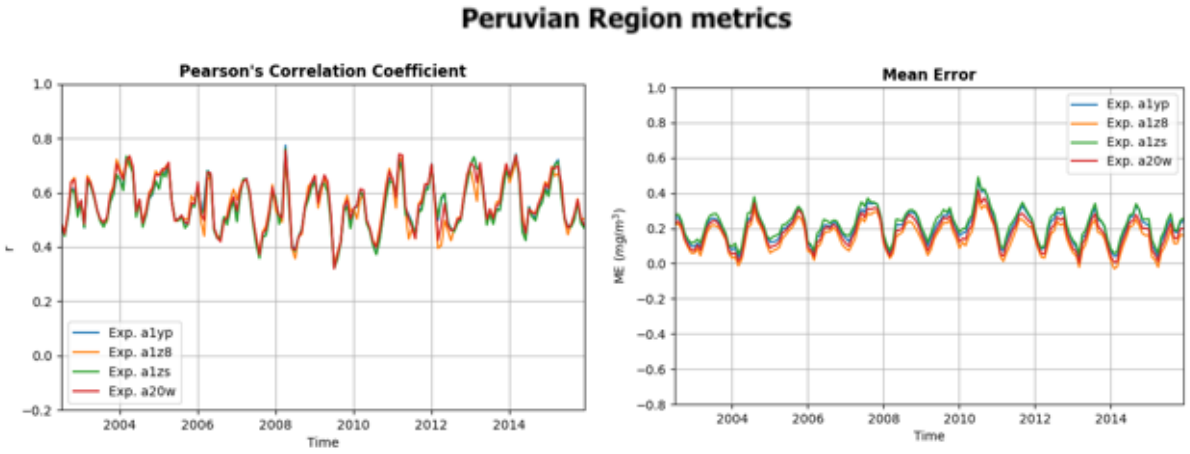

Fig. 14. Time series of the spatial metrics for the Peruvian region for each experiment.

3. *Equatorial Atlantic Region*

In this region, the greatest differences between the different experiments were found. The variable presents a seasonal pattern with maximum SCC during the northern summer. The model also follows this variability, but with noticeable differences (Fig. 15).

Experiments a1z8 and a20w overestimate the SCC during the summer months. On the other hand, experiments a1yp and a1zs overestimate the variable during the whole period considered. This is reflected in the temporal metrics of the averaged chlorophyll. As in other regions, the first and the third experiments carry out a worse simulation of the SCC, being the second experiment the one which better predicts the variable. The obtained metrics are shown in Table 6.

Table 6. Metrics of the temporal mean SCC series for each experiment for the Equatorial Atlantic region.

Experiment	r	RMSE (mg/m^3)
1. a1yp	0.78	0.15
2. a1z8	**0.86**	**0.13**
3. a1zs	0.76	0.15
4. a20w	0.83	0.14

In line with these results, the time series of the spatial metrics show that the first and third experiments predict markedly worse the SCC temporal variability, with lower values of the correlation coefficient and higher mean absolute error than the second and forth experiments (Fig. 16). Experiment a1z8 is again the most accurate one. Although the correlation coefficient series present a lot of noise, it shows that the minimum r values occur during the low SCC months, and the other way round. This is also evidenced by the mean absolute error series.

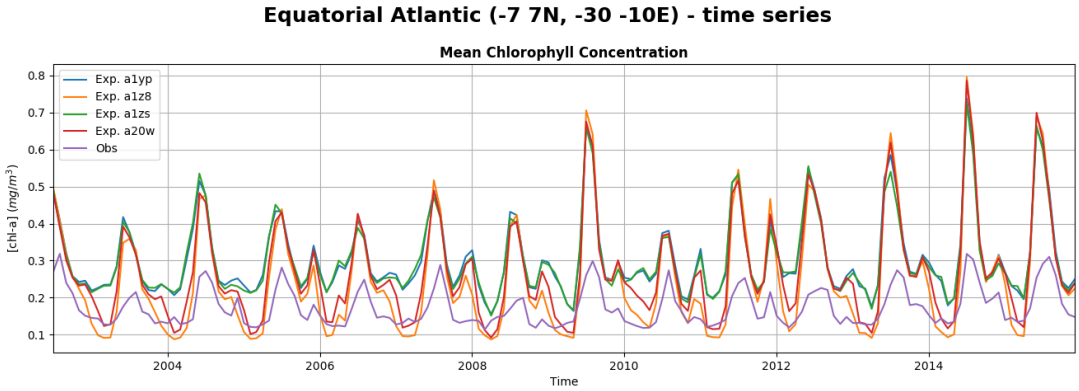

Fig. 15. Time series of the spatial mean SCC in the Equatorial Atlantic region for each experiment and observations.

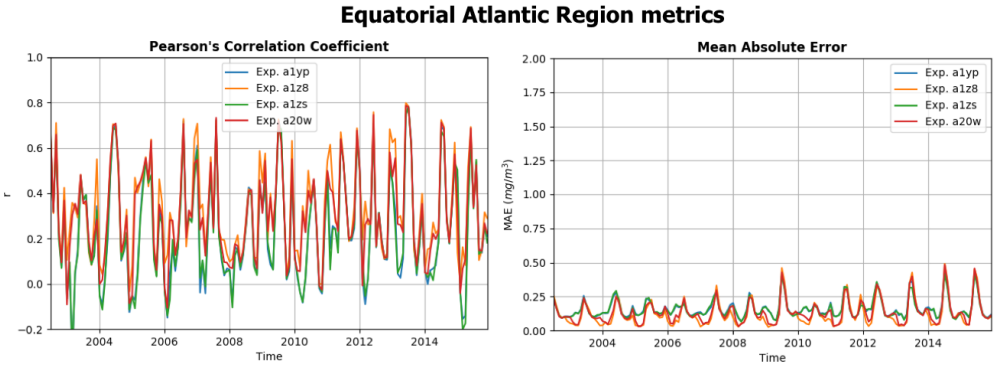

Fig. 16. Time series of the spatial metrics for the Equatorial Atlantic region for each experiment.

4. *Namibian Region*

The observed surface chlorophyll concentration in the Namibian region presents a seasonal pattern similar to that of a northern hemisphere region, with maximum values during the central months of the year. This variability is slightly displaced in the simulations (Fig. 17), with the maximum and minimum values of SCC one or two months after the ones observed. However, the model carries out a reasonable temporal simulation of the averaged variable along this area, with a Pearson's correlation coefficient of 0.54.

There is a noteworthy maximum value of chlorophyll concentration during August 2010, not captured by the model.

The spatial correlation is shown in Fig. 18, with significantly high r values between 0.5 and almost 0.8. This shows that the spatial distribution of the simulated SCC is quite consistent with the satellite data, being the region that presents the highest minimum spatial correlation value along the analysed period. Experiment a1z8 presents, in this case, lower correlation with the observations than the other experiments.

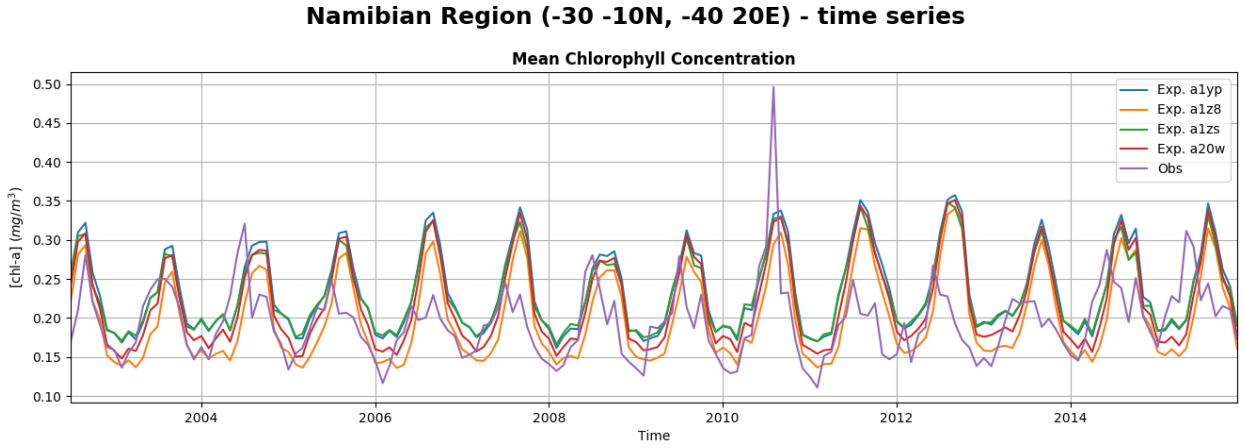

Fig. 17. Time series of the spatial mean SCC in the Namibian region for each experiment and observations.

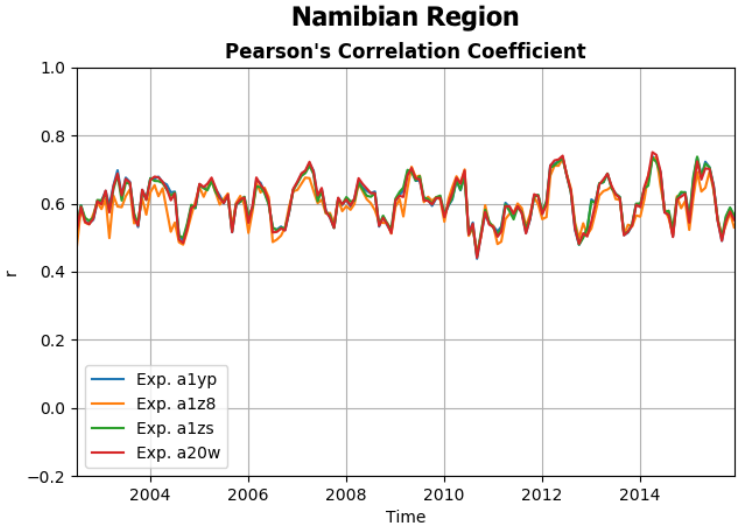

Fig. 18. Time series of the spatial metrics for the Namibian Region for each experiment.

5. *Southern Ocean Regions*

These three regions (Southern Atlantic region, Southern Indian region and Southern Pacific region), spanning exactly the same latitudinal fringe, were included due to the similar pattern they expose. In all of them, specially in the Atlantic and Indian oceans, the model simulates the maximum and minimum SCC periods a few months before it really takes place, as showed by the observations. None of the experiments improve the predictions in this regard, as there are practically no differences between them.

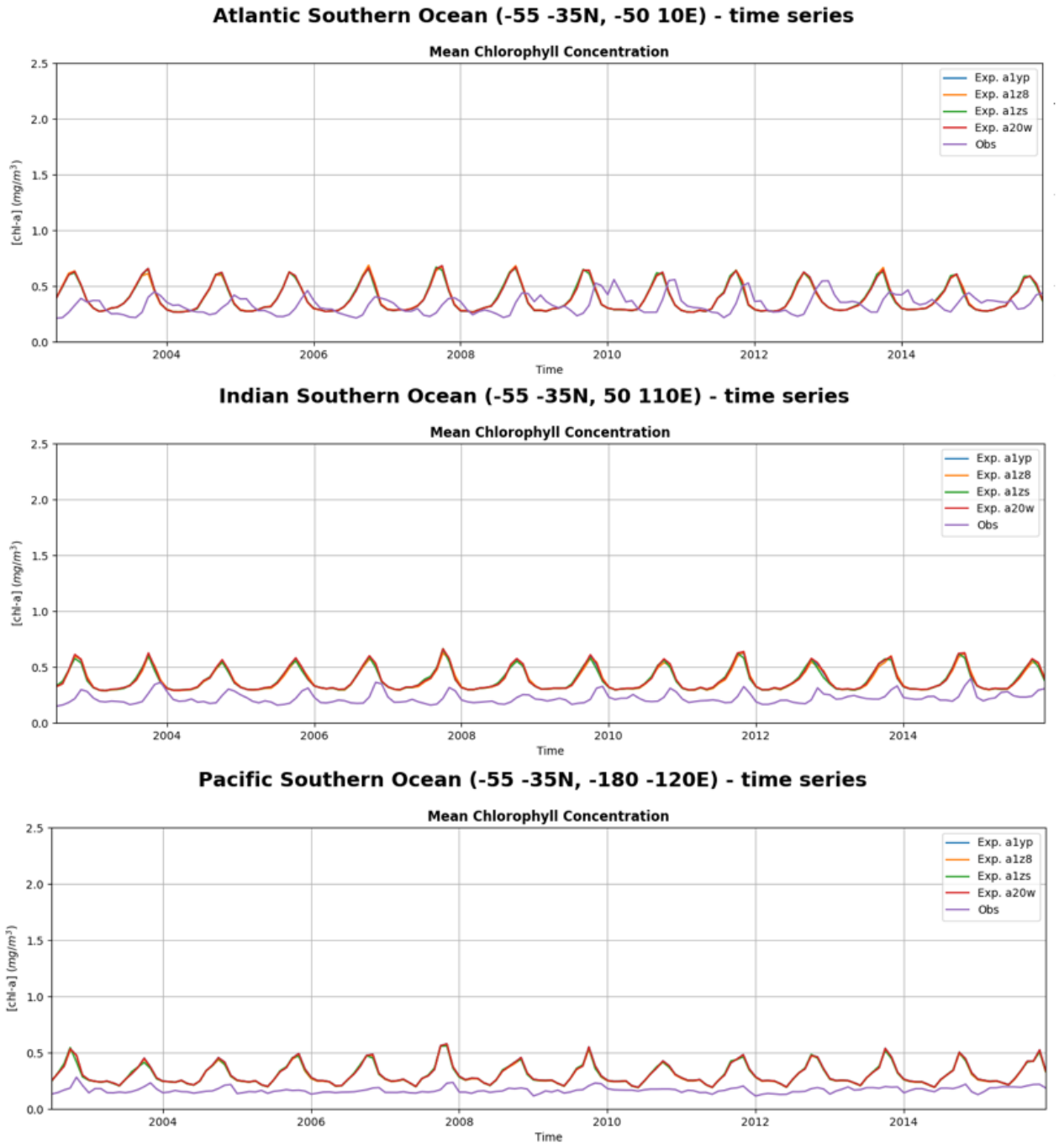

Fig. 19. Time series of the spatial mean SCC in three Southern Ocean regions (Atlantic, Indian and Pacific) for each experiment and observations.

Correlation maps

Finally, a temporal correlation analysis was done for every point of the grid. The Pearson's correlation coefficient was calculated for the temporal series (162 months) of each point between the four experiments and the observations separately, obtaining four correlation maps (Figs. 20, 21, 22 and 23).

To this end, the seasonal cycle was removed from every point temporal series, both in the observations and in the simulations. The procedure was to subtract from each monthly SCC value the average of that specific month in the whole period. The correlation was then calculated for the anomalies series. This was done to obtain the real skill of the model in predicting interannual anomalies of SCC, assuming that the seasonal cycle had to be captured in the simulations.

Contrary to the previous analysis, the correlation maps do not show significant differences between the experiments.

The most remarkable regions of skill for the four experiments are: the mid-latitude northern Atlantic, the western part of the mid-latitude southern Atlantic, a great part of the Indian Ocean and the tropical region of the western Pacific Ocean.

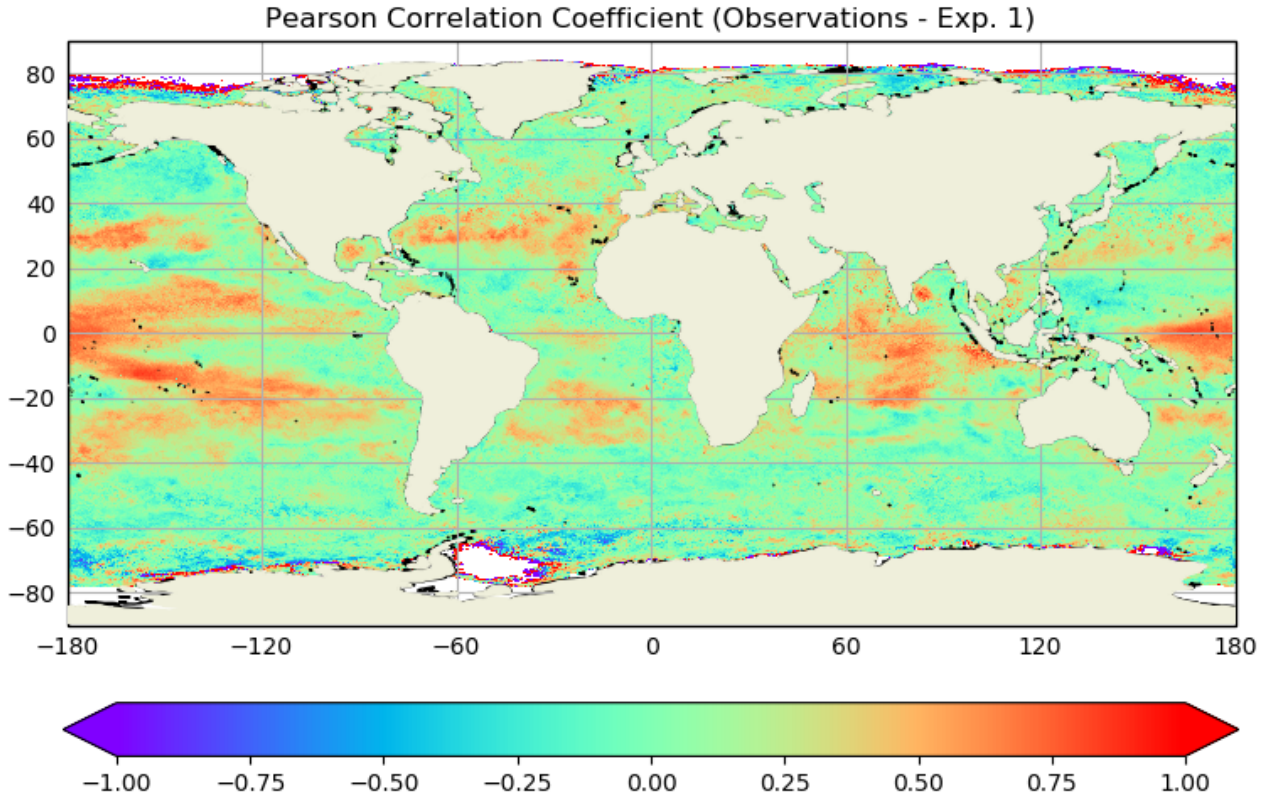

Fig. 20. Correlation map for the experiment a1yp.

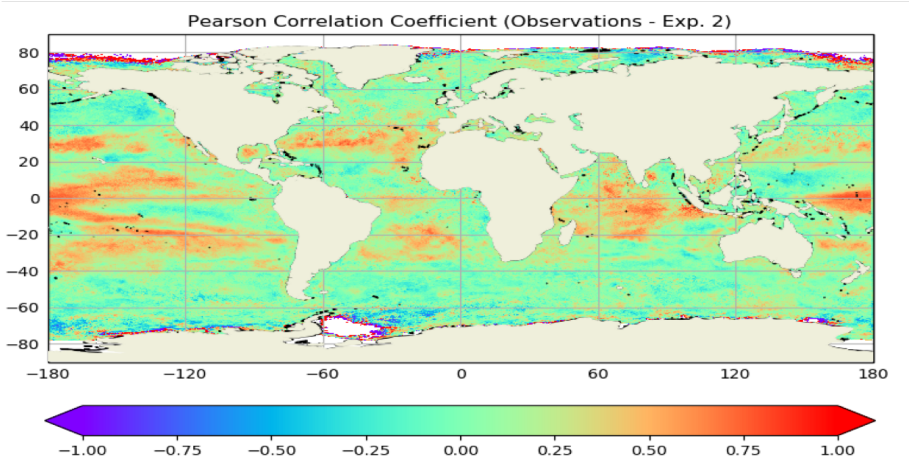

Fig. 21. Correlation map for the experiment a1z8.

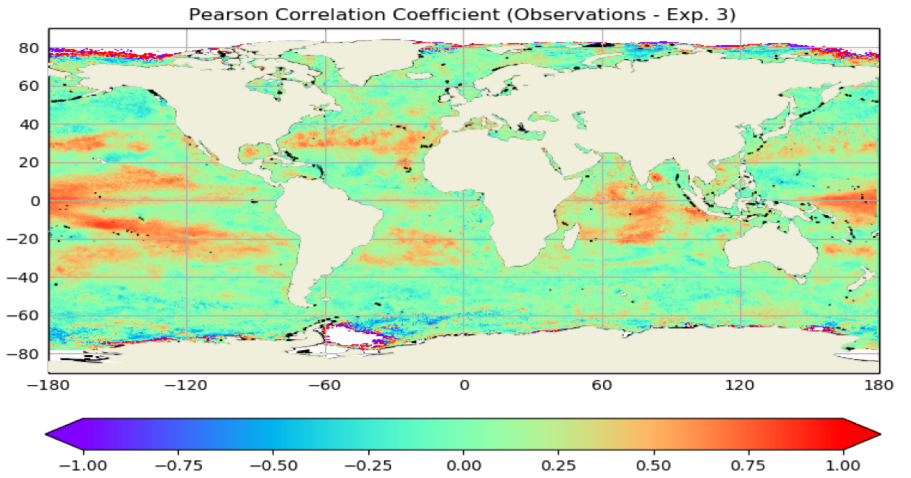

Fig. 22. Correlation map for the experiment a1zs.

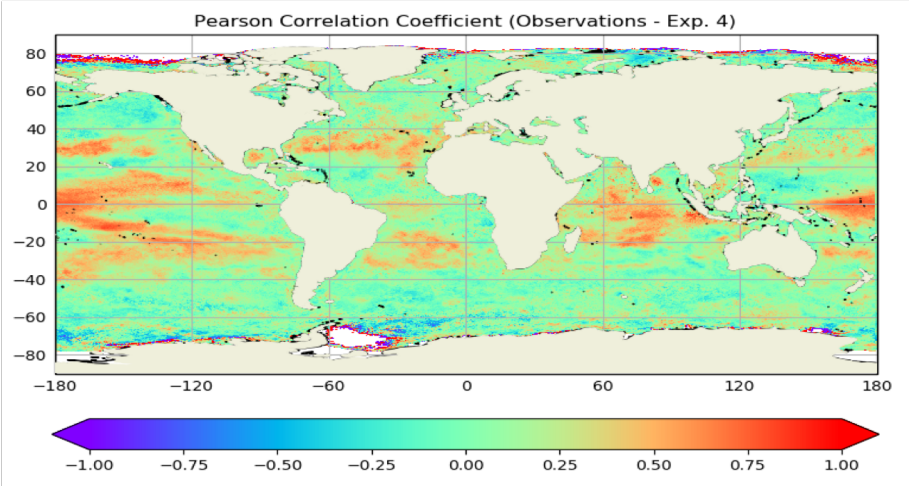

Fig. 23. Correlation map for the experiment a20w.

Discussion

Regarding the large-scale analysis, the model correctly simulates the seasonal cycle of the global mean SCC ($r = 0.68$), with maximum values during the northern summer, although this oscillation is less pronounced in the simulations, as shown in Figs. 6 and 7. This could be related with the spatial homogeneity of the simulated SCC fields (Fig. 6): the model overestimates the low SCC regions, this is, the open ocean, that has less seasonal variability, and underestimates the high SCC regions, generally coastal areas, which markedly vary over the year. As a result, the chlorophyll predictions present lower spatial and temporal fluctuations. On the other hand, high spatial variances of satellite data reflect the patched distribution of chlorophyll *a* over the oceans.

As studied by Yoder et al. (1993), the northern hemisphere shows higher SCC values than the southern hemisphere. Despite the larger ocean area in the SH, higher mean annual concentrations of SCC in the NH lead to similar hemispherical chlorophyll contributions. Furthermore, the observed global seasonal cycle coincides with that of the NH ($r = 0.98$), which indicates that seasonal oscillations in the overall SCC are given by the NH seasonality. This pattern leads to a better simulation of the variable in the NH ($r = 0.54$). In the SH, the simulations considerably overestimate the seasonality of the variable ($r = 0.43$), with marked chlorophyll peaks during the austral summer. Satellite measurements show a much more homogeneous SCC field in time for this hemisphere. This could be a result of the larger open ocean area, which, as stated above, has lower variability during the year.

The global increase in the SCC observed in the last years of the analysed period, not captured by the model, has its origin in the NH, concretely in the North Atlantic region, as clearly exposed in Fig. 12. This could be due to several factors, such as the North Atlantic Oscillation, variability in the AMOC [13], the sea surface temperature or the ocean-mixing strength, as indicated by Li et al. (2016). These and other potential drivers could be examined in detail in future researches, in order to improve the model's response in this kind of events.

The equatorial region is the best simulated by the model ($r = 0.75$). In addition, it is the only one that presents noticeable differences between the experiments in the large-scale analysis. This could be related with the no-nudging area established in each experiment, where the solutions are not guide towards the observations, as in the nudged regions. The one with a wider no-nudging fringe (15ºS-15ºN), experiment a1z8, is the one that better simulates the variable near the equator, as shown by the root mean square error in Table 4. This fact is supported by the analysis of the Peruvian and the Equatorial Atlantic regions, where the experiment a1z8 is also the most accurate in predicting the SCC.

As studied by Skyllas (2018), the model showed a tendency to move forward the seasonality of the variable, in this case in the southern hemisphere (Fig. 19). The mechanisms behind this pattern could be numerous and a deeper assessment should be carried out to examine its origin.

Finally, a cursory analysis of another biogeochemical variable was carried out. The nitrate (NO_3) field is closely related with chlorophyll concentration as it is one of the main nutrients needed by phytoplankton. In accordance with the SCC simulations, Fig. 24 shows that the experiments with a wider no-nudging band around the equator (a1z8 and a20w) better simulate the surface NO_3 field. Driving the solution towards a reference state in this region generates strong vertical velocities. This leads to an overestimated transport of nutrients to the ocean surface, therefore, to higher chlorophyll concentration values.

[13] Atlantic Meridional Overturning Circulation.

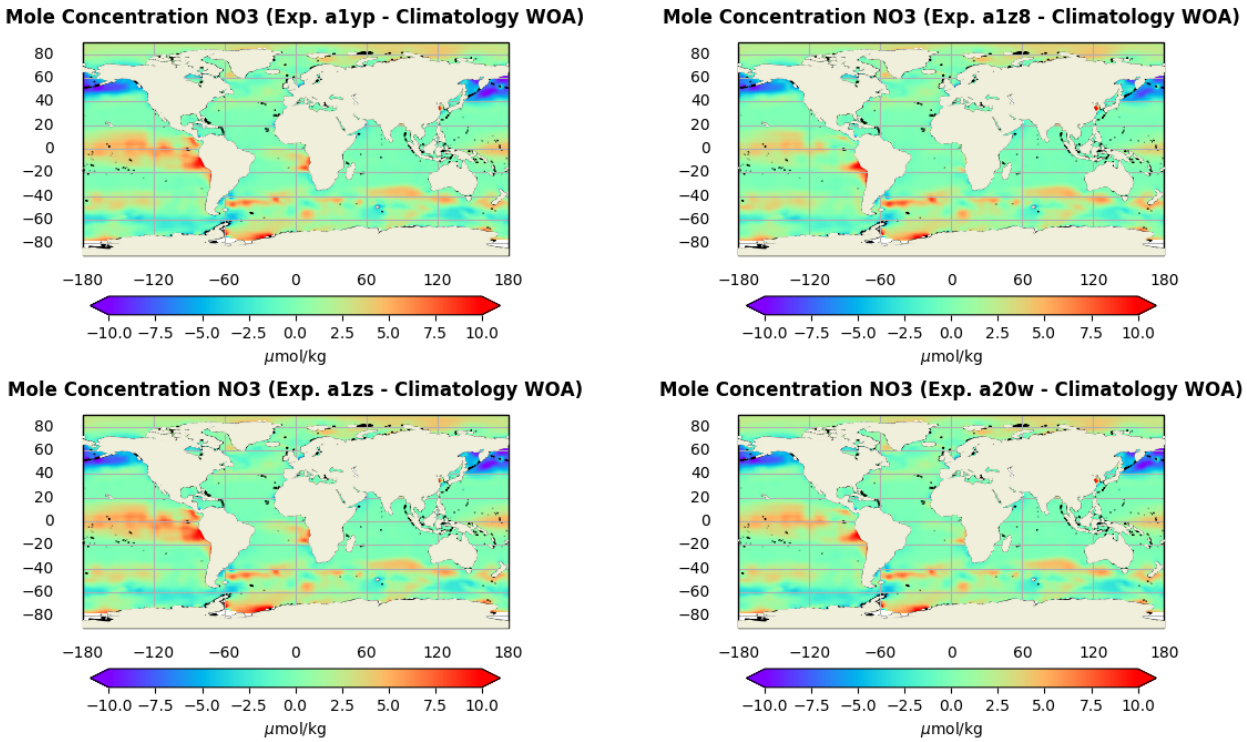

Fig. 24. Difference between the NO_3 field for each experiment and the World Ocean Atlas climatology.

Conclusions

Near-term climate prediction is becoming a widely researched branch of Earth sciences. Earth system models are the state-of-the-art tools available to this end. However, the assessment of the capacity of the simulations to predict biogeochemical variables remains almost unexplored. In this study, four different experiments from the ocean component of EC-Earth, NEMO, were evaluated in order to assess the accuracy of the simulations derived from this model and to find the best set of initial conditions for predictions of ocean biogeochemistry. The main results obtained from this validation are set out below:

- The model adequately simulates the global seasonal cycle of SCC, that has its origin in the northern hemisphere.

- The simulated variable is more homogeneous than satellite observations, both spatially and temporally.

- The model did not capture a significant increase in the SCC during the last years of the analysed period. This could be due to deficiencies in other components of the model by not predicting specific processes that regulate the SCC.

- This SCC increase comes from the North Atlantic region, where phenomena like NAO or the AMOC variability have direct influence over the chlorophyll fields, as studied by Li et al. (2016).

- The NH presents higher values of SCC, a stronger seasonal pattern and better agreement with the observations than the SH. The austral hemisphere has a slight seasonal cycle, largely overestimated by the model. None of them present noticeable differences between the four experiments.

- The equatorial region shows the most accurate predictions for the temporal series of the spatial mean SCC, regarding the large-scale analysis.

- In the equatorial region, the experiment a1z8 is the one that best fits the chlorophyll *a* measurements, followed by the experiment a20w. This fact is confirmed by the Peruvian and the Equatorial Atlantic regions. These differences have its origin in the no-nudging fringe around the equator left in each experiment.

- The three Southern Ocean regions show the same pattern: the model moves forward the seasonality of the variable a few months.
- The improvement in the second experiment is not reflected in the correlation maps, where the seasonal cycle was removed before estimating the correlation coefficients.
- The NO_3 simulations confirm that the experiments a1z8 and a20w represent better initial conditions for predictions of ocean biogeochemistry than the other two experiments.

Acknowledgements

I would like to thank my supervisors Irene Polo Sánchez and Raffaele Bernardello for sharing their knowledge and guiding me through this project. I would also want to thank Pablo Ortega Montilla for his time and always interesting contributions.

References

Li, H., Ilyina, T., Müller, W.A. & Sienz, F. (2016). Decadal predictions of the North Atlantic CO_2 uptake. *Nature Communications*. doi: 10.1038/ncomms11076.

Doblas-Reyes F.J., Andreu-Burillo, I., Chikamoto, Y., García-Serrano, J., Guemas, V., Kimoto, M., Mochizuki, T., Rodrigues, L.R.L. & van Oldenborgh, G.J. (2013). Initialized near-term regional climate change prediction. *Nature Communications*. doi: 10.1038/ncomms2704.

Falkowski, P. (1996). The role of phytoplankton in the global carbon cycle. S.It.E. Atti, 17, 3–6.

Pérez-Arvizu, E., Aragón-Noriega, A. & Espinosa-Carreón, L. (2013). Variabilidad estacional de la clorofila a y su respuesta a condiciones El Niño y La Niña en el Norte del Golfo de California. *Revista de Biología Marina y Oceanografía*. Vol. 48, Nº 1. doi: 10.4067/S0718-19572013000100011.

Winder, M. & Cloern, J. (2010). The annual cycles of phytoplankton biomass. *The Royal Society Publishing*. doi: 10.1098/rstb.2010.0125.

Lee. K.W., Yeh, S.W., Kug, J.S. & Park, J.Y. (2014). Ocean chlorophyll response to two types of El Niño events in an ocean-biogeochemical coupled model. *J. Geophys. Res Oceans, 119, 933-952*. doi: 10.1002/2013JC009050.

Séférian, R., Bopp, L., Gehlen, M., Swingedouw, D., Mignot, J. Guilyardi, E. & Servonnat, J. (2013). Multiyear predictability of tropical marine productivity. www.pnas.org/cgi/doi/10.1073/pnas.1315855111.

Gordon, H. & Wang, M. (1994). Retrieval of water-leaving radiance and aerosol optical thickness over the oceans with SeaWiFS: a preliminary algorithm. *University of Miami*. doi: 0003-6935/94/030443-10$06.00/0.

O'Reilly, J., Maritorena, S., Mueller, J., Strutton, P., Cota, G., Phinney, D. & Culver, M. (2000). Ocean color chlorophyll a algorithms for SeaWiFS, OC2 and OC4: Version 4. *NASA Technical Memorandum*. 2000-206892.

Hu, C., Lee, Z. & Franz, B. (2012). Chlorophyll a algorithms for oligotrophic oceans: a novel approach based on three-band reflectance difference. *J. Geophys. Res*. doi: 10.1029/2011JC007395.

Chen, J., Cui, T., Zhang, M. & Wen, Z. (2013). A review of some important technical problems in respect of satellite remote sensing of chlorophyll-a concentration in coastal waters. *IEEE Journal of selected topics in applied Earth observations and remote sensing*. doi: 10.1109/JSTARS.2013.2242845.

Gerber, F., Furrer, R., Schaepman-Strub, G., de Jong, R. & Schaepman, M. (2016). Predicting missing values in spatio-temporal satellite data. *University of Zurich*.

Donners, J., Basu, C., Mckinstry, A. & Asif, M. (2012). Performance Analysis of EC-Earth 3.1.

Aumont, O., Ethé, C., Tagliabue, A., Bopp, L. & Gehlen, M. (2015). PISCES-v2: an ocean biogeochemical model for carbon and ecosystems studies. *Geoscientific Model Development*. doi: 10.5194/gmd-8-2465-2015.

Otte, T. (2007). The impact of nudging in

the Meteorological Model for Retrospective Air Quality Simulations. Part II: Evaluating collocated meteorological air quality observations. *Journal of Applied Meteorology and Climatology*. p: 1868-1887.

Ortega, P., Guilyardi, E., Swingedouw, D., Mignot, J. & Nguyen, S. (2017). Reconstructing extreme AMOC events through nudging of the ocean surface: a perfect model approach. *Clim Dyn*. doi: 10.1007/s00382-017-3521-4.

Yoder, J., McClain, C., Feldman, G. & Esaias, W. (1993). Annual cycles of phytoplankton chlorophyll concentrations in the global ocean: a satellite view. *American Geophysical Union*. doi: https://doi.org/10.1029/93GB02358.

Echevin, V., Aumont, O., Ledesma, J. & Flores, G. (2008). The seasonal cycle of surface chlorophyll in the Peruvian upwelling system: a modelling study. *Progress in Oceanography*. doi: 10.1016/j.pocean.2008.10.026.

Skyllas, N. (2018). Evaluation of NEMO-PISCES v2 biogeochemical model with field data from a north-south gradient in the Northeast Atlantic Ocean. *Utrecht University*.